Energy-level shifts and the decay rate of an atom in the presence of a conducting wedge

Zahra Mohammadi and Fardin Kheirandish*
Department of Physics, Faculty of Science, University of Isfahan, Isfahan, Iran
(Received 2 February 2015; revised manuscript received 7 July 2015; published 14 December 2015)

In the present article explicit expressions for the decay rate and energy-level shifts of an atom in the presence of an ideal conducting wedge, two parallel plates, and a half sheet are obtained in the framework of the canonical quantization approach. The angular and radial dependences of the decay rate for different atomic polarizations of an excited atom and also of the energy-level shifts are depicted and discussed. The consistency of the present approach in some limiting cases is investigated by comparing the relevant results obtained here to the previously reported results.

DOI: 10.1103/PhysRevA.92.062118 PACS number(s): 12.20.Ds

I. INTRODUCTION

An immediate consequence of the quantization of an electromagnetic field is the occurrence of the field fluctuation in the vacuum state. The effect of vacuum fluctuations on atomic systems leads, for example, to observable phenomena such as spontaneous emission or atomic energy-level shifts [1,2]. These radiative properties are explained as the reaction of an atom to the existence of the zero-point field.

In quantum field theory the existence of any modification in the presence of an environment is an interesting subject that has been widely studied. In principle, the calculations of these radiation properties in the presence of an environment therefore become the search for a quantized electromagnetic field in the presence of material fields in order to have a correct picture of fluctuation-induced effects on atomic systems. Therefore, we should quantize the electromagnetic field in the presence of material fields [3–6] in order to have the explicit form of the field operators. A similar situation arises in static or dynamical Casimir effects, which are a consequence of constrained vacuum fluctuations imposed by boundary conditions on macroscopic objects [7]. The presence of a boundary surface gives rise to alterations of vacuum field fluctuations and accordingly the energy-level shifts and the decay rate of atomic systems change as the atom changes its position with respect to boundary surfaces [8–15]. Formalisms using different methods for only the dipole decay rate were explained in other works [16–18]. In this paper we use another approach that describes both the decay rate and the energy-level shifts of an atom in terms of the imaginary part of the dimensionless vector potential Green's function. We will see that for the dipole decay rate, agreement with the results of the other approaches is found.

As expected, the deexcitation process for different wedges can also occur for an atom inside a wedge. This phenomenon suggests that the work presented here is applicable to the area of quantum information processing and the system might serve as a qubit [19].

In the present work we investigate the decay rate and energy-level shift of an atom in the presence of a conducting wedge in the framework of canonical quantization based on previous works [4–6]. The main ingredients of the formalism are the components of the Green's tensor of the electromagnetic field in the presence of material fields. We have analyzed various important limiting cases such as a plane sheet, two parallel plates, and a half sheet.

The paper is organized as follows. The basic formulation is presented in Sec. II. In Sec. III the decay rate and the energy-level shifts of an atom in the presence of a perfectly conducting wedge is investigated. In Sec. IV the spontaneous emission of an atom located between parallel plates (the limiting case of a wedge) is investigated. In Sec. V the radiation properties of an atom in the presence of a half sheet (the limiting case of a wedge) are studied.

II. BASIC FORMULAS

A. Effective products for the electric field

In a general, linear, isotropic magnetodielectric medium, the electric field satisfies the equation [6]

$$\boldsymbol{\nabla}\times\left(\frac{1}{\mu}\boldsymbol{\nabla}\times\mathbf{E}\right)-\frac{\omega^2}{c^2}\epsilon\mathbf{E}=\mu_0\omega^2\mathbf{P}^N+i\mu_0\omega\boldsymbol{\nabla}\times\mathbf{M}^N, \quad (1)$$

where $\mathbf{P}^N(\mathbf{r},\omega)$ and $\mathbf{M}^N(\mathbf{r},\omega)$ are polarization and magnetization noise fields and $\epsilon(r,\omega)$ and $\mu(r,\omega)$ are dimensionless permittivity and permeability of the medium, respectively. The constant μ_0 is the permeability of the vacuum. The Green's dyadic $\mathbf{D}(\mathbf{r},\mathbf{r}';\omega)$ of Eq. (1) satisfies

$$\boldsymbol{\nabla}\times\left(\frac{1}{\mu}\boldsymbol{\nabla}\times\mathbf{D}\right)-\frac{\omega^2}{c^2}\epsilon\mathbf{D}=\mu_0\omega^2\mathbf{1}\delta(\mathbf{r}-\mathbf{r}'). \quad (2)$$

Let us assume for simplicity that the medium is nonmagnetic. Then from Eq. (2) the electric field $\mathbf{E}(\mathbf{r},\omega)$ can be written in terms of the polarization noise $\mathbf{P}^N(\mathbf{r},\omega)$ as

$$\mathbf{E}(\mathbf{r},\omega)=\int d\mathbf{r}'\mathbf{D}(\mathbf{r},\mathbf{r}';\omega)\cdot\mathbf{P}^N(\mathbf{r}',\omega). \quad (3)$$

The Green's dyadic in real time can be obtained from the Fourier transform

$$\mathbf{D}(\mathbf{r},\mathbf{r}';\tau)=\int_{-\infty}^{+\infty}\frac{d\omega}{2\pi}e^{-i\omega\tau}\mathbf{D}(\mathbf{r},\mathbf{r}';\omega), \quad (4)$$

where $\tau=t-t'$. Equation (3) in space-time can be written as [20–22]

$$\mathbf{E}(\mathbf{r},t)=\iint d\mathbf{r}'dt'\mathbf{D}(\mathbf{r},\mathbf{r}';t-t')\cdot\mathbf{P}^N(\mathbf{r}',t'). \quad (5)$$

*fkheirandish@yahoo.com

The quantum mechanical monochromatic expectation values are related to the Green's dyadic through [23]

$$\langle E_i(\mathbf{r})E_j(\mathbf{r}')\rangle_\omega = \frac{\hbar\mu_0}{\pi}\omega^2 D_{ij}(\mathbf{r},\mathbf{r}':\omega), \tag{6}$$

$$\langle H_i(\mathbf{r})H_j(\mathbf{r}')\rangle_\omega = \frac{\hbar}{\pi\mu_0}\lim_{\mathbf{r}'\to\mathbf{r}}\frac{1}{\mu^2(\mathbf{r},\omega)} \times [\overrightarrow{\nabla}\times\mathbf{D}(\mathbf{r},\mathbf{r}';\omega)\times\overleftarrow{\nabla}']_{ij}. \tag{7}$$

Here we are considering the medium as a perfect conductor, so we solve Eq. (2) in vacuum with the restriction that the field components on boundaries should satisfy perfect conductor boundary conditions.

B. Decay rate of an initially excited atom

To find the radiative properties of an atom in the presence of a boundary surface we need the explicit form of the field operators. Finding the explicit form of these operators in a general geometry, due to the intricate structure of field expressions, is a very difficult task or even impossible if we are not invoking numerical calculations. However, we can find an alternative approach to find the radiative properties of an atom without dealing with the explicit forms of the field operators. In this approach we try to find the electromagnetic dyadic tensor satisfying all boundary conditions imposed on the boundaries. Here the boundary that we are interested in is an ideal conducting wedge that can be transformed to a plane, two parallel plates, and a half plane as limiting cases. Here a very short introduction to the derivation of the basic formulas is given and the details of the calculations can be found in, for example, [24].

Up to the dipole approximation, the decay rate of an excited atom is given by Fermi's golden rule

$$\Gamma = \frac{2\pi}{\hbar^2}\sum_f |\langle f|\mathbf{d}_0\cdot\hat{\mathbf{E}}(\mathbf{r}_0,t)|0\rangle|^2\delta(\omega_f-\omega_0), \tag{8}$$

where $\mathbf{r}_0$, ω_0, and $\mathbf{d}_0$ are the position, transition frequency, and dipole moment of the atom, respectively. The kets $|f\rangle$ and $|0\rangle$ are the final and vacuum states of the electromagnetic field, respectively. If we decompose the electric field into positive and negative frequency parts and make use of the fluctuation-dissipation theorem and Kubo's formula [25]

$$\langle 0|\hat{E}^+_\alpha(\mathbf{r},\omega)\hat{E}^-_\beta(\mathbf{r}',\omega')|0\rangle = 2\hbar\omega^2\mathrm{Im}D_{\alpha\beta}(\mathbf{r},\mathbf{r}',\omega)\delta(\omega-\omega'), \tag{9}$$

we can find the decay rate of an initially excited atom as [24]

$$\Gamma = \frac{2}{\hbar}\omega^2\mathrm{Im}[\mathbf{d}_0\cdot\mathbf{D}(\mathbf{r}_0,\mathbf{r}_0,\omega)\cdot\mathbf{d}_0], \tag{10}$$

where $\mathbf{D}(\mathbf{r}_0,\mathbf{r}_0,\omega)$ is the Green's tensor of the electromagnetic field in the presence of boundaries with the components $D_{\alpha\beta}$ appearing in (9). For dimensional considerations, usually the Green's tensor is written in terms of the dimensionless Green's tensor $\mathscr{D}_{\alpha\beta}(\mathbf{r},\mathbf{r}',\omega)$ as

$$D_{\alpha\beta}(\mathbf{r},\mathbf{r}',\omega) = \frac{\omega}{4\pi\varepsilon_0 c^3}\mathscr{D}_{\alpha\beta}(\mathbf{r},\mathbf{r}',\omega), \tag{11}$$

where ε_0 and c are the permittivity and the velocity of light in free space, respectively. Throughout the paper the summation convention is assumed, i.e., repeated indices are summed over the three Cartesian coordinates x,y,z. In the absence of boundaries or material fields, the decay rate of an excited atom turns out to be

$$\Gamma_0 = \frac{d_0^2\omega_0^3}{3\pi\varepsilon_0\hbar c^3}. \tag{12}$$

By inserting Eqs. (11) and (12) into (10), we finally find

$$\Gamma_\alpha = \tfrac{3}{2}\Gamma_0\mathrm{Im}[\mathscr{D}_{\alpha\alpha}(\mathbf{r}_0,\mathbf{r}_0,\omega_0)], \tag{13}$$

where the subscript α refers to the different orientations of the dipole moment of the atom. Although it is generally understood that spontaneous emission of an excited atom is a pure quantum mechanical effect and requires a quantum mechanical treatment, according to the correspondence principle, there should be a correspondence between the decay rate of an atom and the energy dissipation by a classical dipole in the same geometry in large quantum numbers. Actually, the classical equation for energy dissipation by a dipole based on Poynting's theorem is given by [26]

$$\frac{dW}{dt} = \frac{\omega_0^3}{2\varepsilon}\mathrm{Im}[\mathbf{d}_0\cdot\mathbf{D}(\mathbf{r}_0,\mathbf{r}_0,\omega)\cdot\mathbf{d}_0]. \tag{14}$$

The mathematical similarity between Eqs. (10) and (14) is inspiring and up to a scale, both Eqs. (10) and (14) depend on geometrical components involved in the Green's tensor similarly, so we expect a similar behavior when plotting these equations in geometrical components. In a simple experimental setup discussed in [27], a classical analog of a quantum electrodynamics effect was investigated. In this experiment the fractional power loss for a classical dipole antenna located on the central symmetry line of a wedge-shaped cavity was obtained and a comparison of the results with those obtained here from a quantum treatment shows agreement up to a scale as expected. For an experimental investigation of a classical dipole antenna between parallel mirrors the reader is referred to [28].

C. Energy-level shift

Following a general formalism for calculating the energy-level shift of an atom in the presence of a boundary surface [24,29,30], we can find the contribution of boundary surfaces to the energy-level shift as

$$\Delta E_n = \frac{ze^4\hbar}{32\pi^3\varepsilon_0^2c^3m^2}\int_0^{\frac{mc}{\hbar}}\frac{q}{q^2+\gamma^2}Q_{\alpha\beta}\mathrm{Im}[\mathscr{D}_{\alpha\beta}(\mathbf{r_0},\mathbf{r_0},\omega)]dq, \tag{15}$$

where $q=\omega/c$ and

$$Q_{\alpha\beta} = -\langle n|\frac{\partial^2}{\partial x_\alpha\partial x_\beta}\frac{1}{R}|n\rangle,$$
$$\gamma = |E_n - E_m|_{\mathrm{av}}/c\hbar = 17.8R_\infty/c\hbar. \tag{16}$$

The constant R_∞ is the Rydberg unit of energy. The cutoff frequency $mc/\hbar$ in Eq. (15), which is the Compton wavelength of the electron, is needed due to the validity of the dipole approximation [24]. The main ingredient of the basic formulas

(13) and (15) is the dimensionless Green's tensor. In the next section the decay rate of an initially excited atom and also the energy-level shift are obtained for an atom located at an arbitrary point inside a perfectly conducting wedge.

III. PERFECTLY CONDUCTING WEDGE

A. Decay rate

Consider an initially excited atom located at an arbitrary point P inside an infinite wedge with perfect conducting walls and the apex angle α (Fig. 1). Due to the symmetry along the z component, the point P is determined by (r_0,θ_0) in the polar coordinates system. The Green's tensor in the presence of a wedge with perfect conducting walls is now a textbook problem and the interested reader can find the details of its derivation in, for example, [31–33]. The relevant components in Eq. (13) are the diagonal components $\mathscr{D}_{rr}$, $\mathscr{D}_{\theta\theta}$, and $\mathscr{D}_{zz}$ given in Appendix A.

Using Eqs. (A14)–(A16), the decay rate of an initially excited atom for different polarizations and apex angles is depicted in terms of the distance from the z axis for $\theta_0 = \alpha/2$ (see Fig. 2). The decay rates are normalized to the decay rates in free space Γ_0. Distances are also normalized to wavelength λ. In all of these diagrams when $r_0 \gg \lambda$, i.e., the atom is far away from the axis, the decay rate tends to the free-space decay rate as expected.

For a 90° wedge ($\alpha = \frac{\pi}{2}$), the dimensionless decay rate $\frac{\Gamma_r}{\Gamma_0}$ for an initially excited and radially polarized atom is depicted in Fig. 2 (see curve a). A comparison of the result with the experimental results reported in [27] for a classical dipole is inspiring.

In Fig. 3 the damping rate for z polarization is depicted in terms of the scaled distance $\frac{r_0}{\lambda}$ for different wedge angles. It can be seen that for distances from the cusp smaller than a certain value determined by the opening angle of the wedge there are regions for which the atom will not decay at all and these suppressions are followed by a sudden jump. It should be noted that here we are considering a perfect conductor; for a good conductor the influence depth δ of the electromagnetic fields inside the conductor is not zero, so the results will be unreliable for distances smaller than or comparable to δ. In a real investigation one should consider real metals. In Fig. 4 the typical behavior of the decay rate in terms of the angle θ for the fixed distance $r_0 = 20\lambda$ from the z axis is depicted for different apex angles α. As expected, these curves are symmetric around the middle point $\theta_0 = \alpha/2$. It is interesting to note that if we consider a wedge with a certain α, for example, $\alpha = \frac{\pi}{3}$ (see Figs. 2 and 4), a change in the dipole orientation changes the decay rate from superradiant to subradiant and vice versa, depending on the location of the atomic dipole.

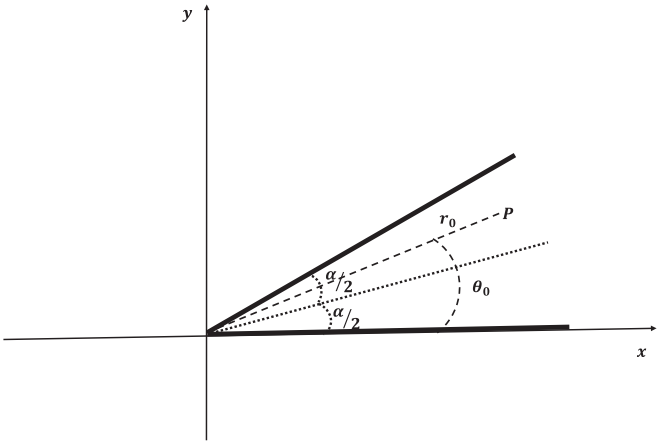

FIG. 1. The atom is located at point P inside a wedge with perfectly conducting walls.

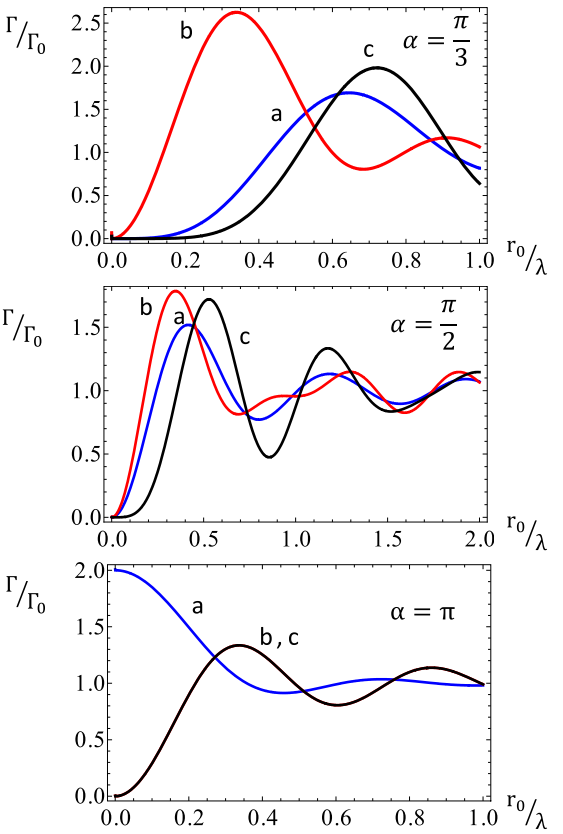

FIG. 2. (Color online) Dimensionless decay rate of an excited atom for three orientations $\frac{\Gamma_r}{\Gamma_0}$ (curve a), $\frac{\Gamma_\theta}{\Gamma_0}$ (curve b), and $\frac{\Gamma_z}{\Gamma_0}$ (curve c) in terms of the dimensionless distance $\frac{r_0}{\lambda}$ from the origin along the symmetry line for the wedges with different α.

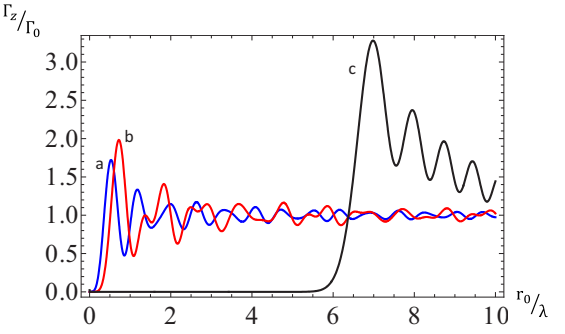

FIG. 3. (Color online) Dimensionless decay rate $\frac{\Gamma_z}{\Gamma_0}$ of the excited atom in terms of the dimensionless distance $\frac{r_0}{\lambda}$ from the origin along the symmetry line for the wedges with different α: $\alpha = \pi/2$ (curve a), $\alpha = \pi/3$ (curve b), and $\alpha = \pi/40$ (curve c).

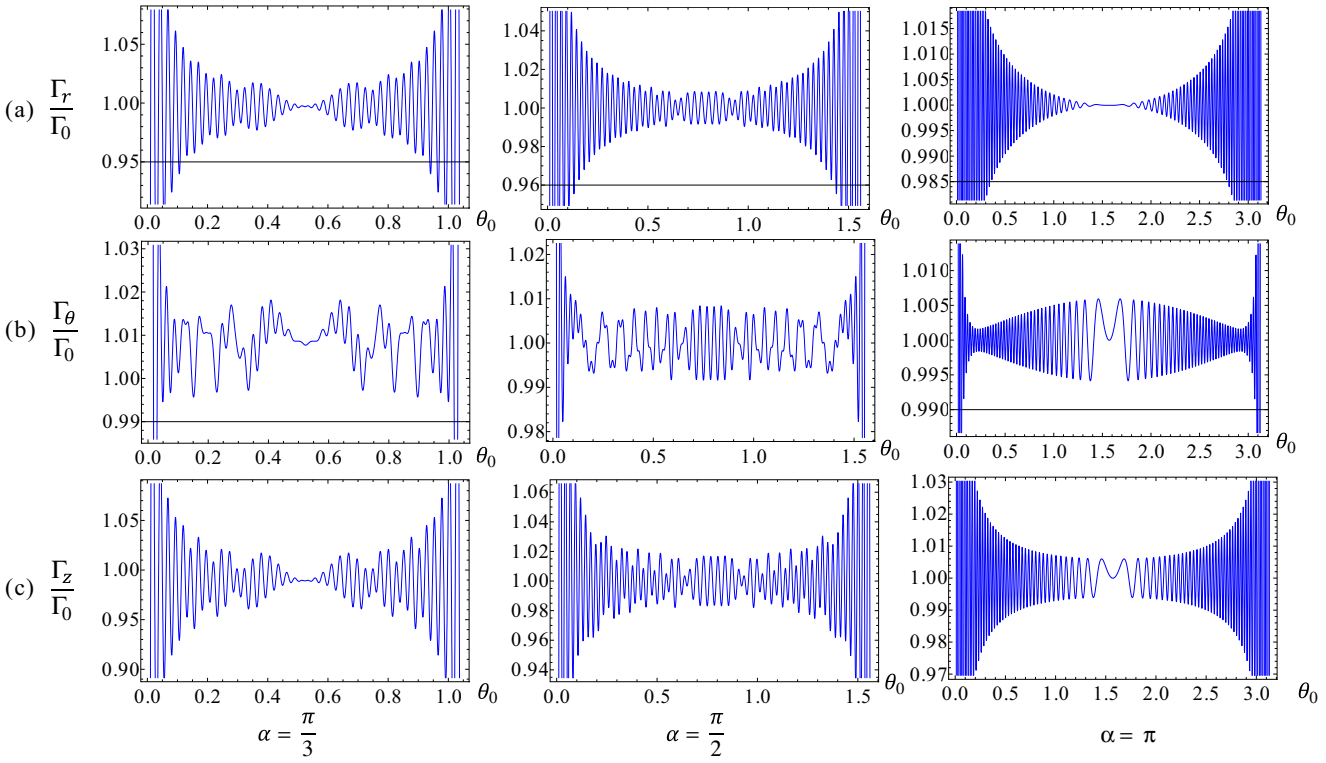

FIG. 4. (Color online) Dimensionless decay rate for three orientations of the polarization of the excited atom (a) $\frac{\Gamma_r}{\Gamma_0}$, (b) $\frac{\Gamma_\theta}{\Gamma_0}$, and (c) $\frac{\Gamma_z}{\Gamma_0}$ in terms of the angle θ_0 and fixed distance $\frac{r_0}{\lambda} = 20$, for $\alpha = \pi/3, \pi/2, \pi$.

For the special case $\alpha = \pi$, the wedge degenerates into a plane sheet. In this case, using Eqs. (A14)–(A16), we find the perpendicular and parallel decay rates as

$$\frac{\Gamma_\parallel}{\Gamma_0} = \frac{\Gamma_z + \Gamma_\theta}{\Gamma_0} = 1 - \frac{3}{2}\left[\frac{\sin(2r_0q)}{(2r_0q)} + \frac{\cos(2r_0q)}{(2r_0q)^2} - \frac{\sin(2r_0q)}{(2r_0q)^3}\right] \quad (17)$$

and

$$\frac{\Gamma_\perp}{\Gamma_0} = \frac{\Gamma_r}{\Gamma_0} = 1 - 3\left[\frac{\cos(2r_0q)}{(2r_0q)^2} - \frac{\sin(2r_0q)}{(2r_0q)^3}\right], \quad (18)$$

which are in agreement with the results reported in [24].

B. Energy-level shift

In this section we find the energy-level shift of an atom placed at an arbitrary point defined by (r_0, θ_0) in Fig. 1. In order to use Eq. (15), we note that the repeated indices are summed over the three Cartesian coordinates $\alpha, \beta = x, y, z$. In Cartesian coordinates the Green's dyadic can be obtained from the one in cylindrical coordinates. For the off-diagonal components, as we expected, due to the symmetry of the problem we find

$$\mathrm{Im}[\mathscr{D}_{\alpha z}(\mathbf{r}_0, \mathbf{r}_0, \omega)] = \mathrm{Im}[\mathscr{D}_{z\alpha}(\mathbf{r}_0, \mathbf{r}_0, \omega)] = 0, \quad (19)$$

in which $\alpha = x, y$ and for two other off-diagonal components it is easy to show that

$$\mathrm{Im}[\mathscr{D}_{xy}(\mathbf{r}_0, \mathbf{r}_0, \omega) + \mathscr{D}_{yx}(\mathbf{r}_0, \mathbf{r}_0, \omega)] \ll \mathrm{Im}\{\mathrm{Tr}[\mathscr{D}(\mathbf{r}_0, \mathbf{r}_0, \omega)]\}, \quad (20)$$

where

$$\mathrm{Tr}[\mathscr{D}] = \mathscr{D}_{xx} + \mathscr{D}_{yy} + \mathscr{D}_{zz} = \mathscr{D}_{rr} + \mathscr{D}_{\theta\theta} + \mathscr{D}_{zz}. \quad (21)$$

Therefore, we can rewrite Eq. (15) as [24]

$$\Delta E_n = \frac{ze^4\hbar}{24\pi^2\varepsilon_0^2 c^3 m^2}|\psi(0)|^2 \times \int_0^{\frac{mc}{\hbar}} \frac{q}{q^2+\gamma^2} \sum_\alpha \mathrm{Im}[\mathscr{D}_{\alpha\alpha}(\mathbf{r_0}, \mathbf{r_0}, \omega)] dq. \quad (22)$$

Using the above equation, we find an expression for the energy-level shifts inside the wedge as given in Appendix B. In Fig. 5 the relative energy-level shifts of an atom inside the wedge are depicted in terms of the distance from the z axis along the symmetry line for different apex angles α. We see that when $\alpha = \frac{\pi}{3}$, at the region near the narrow end of the wedge, the energy-level shifts are much smaller compared to the vacuum case, which means that in this region the atom is more stable in its excited state. For the more realistic case, where there are good conductors instead of ideal ones, the Green's dyadic should be obtained in the presence of matter with a frequency-dependent dielectric function where plasmonic effects are important and the results drastically change near real conductors.

Using Eqs. (6) and (B1), we can define the potential energy ε for a polarizable point particle or an atom as [20]

$$\varepsilon = -\tfrac{1}{2}\alpha(0)\langle \mathbf{E}^2 \rangle, \quad (23)$$

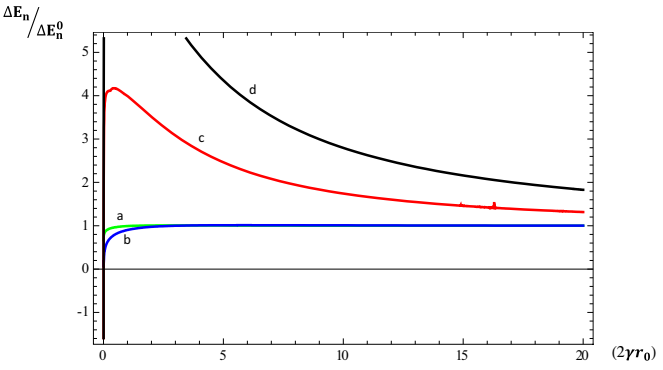

FIG. 5. (Color online) Relative energy-level shifts of an atom inside the wedge in terms of the dimensionless distance $2\gamma r_0$ along the symmetry line of the wedge with different apex angles α: $\alpha = \pi$ (curve a), $\alpha = \pi/3$ (curve b), $\alpha = \pi/50$ (curve c), and $\alpha = \pi/100$ (curve d).

where $\alpha(0)$ is the static electric dipole polarizability of the particle. In compact notation we have

$$\langle \mathbf{E}^2 \rangle = \langle E_r^2 \rangle + \langle E_\theta^2 \rangle + \langle E_z^2 \rangle. \tag{24}$$

One can obtain the expression for the Casimir-Polder energy between the wedge and the atom. The force F is derivable as the gradient of the particle's potential energy. The calculation of this energy was done in [20]. However, a small check of our calculations for the Green's dyadic in the presence of a wedge shows that when $p = 1$ ($\alpha = \pi$) we recover the expected Casimir-Polder result for an atom above an ideal conducting plane

$$\varepsilon(d) = -\frac{3}{32}\frac{\alpha(0)}{\pi^2 d^4}, \tag{25}$$

where $d = r_0 \sin\theta_0$ denotes the distance between the atom and the plane. This is the usual expression for Casimir-Polder interaction [20,34]. For experimental verification see [35].

It should be noted that for the special case $\alpha = 2\pi$, we have $p = \frac{1}{2}$, that is, the wedge degenerates into a half sheet. In this case p is not an integer, so we cannot use Eq. (A4). In Sec. V, using the Green's dyadic reported in [36], we will find the decay rate and energy-level shifts of an atom in the vicinity of an ideal conducting half sheet.

IV. DECAY RATE OF AN ATOM BETWEEN PARALLEL PLATES

There has been increasing interest in the computation of the decay rate of an excited atom located between two parallel plates. Initially, Barton discussed extensively the QED of charged particles between conducting plates [14,15]. Also, Hulet *et al.* reported the experimental inhibited spontaneous emission by a Rydberg atom [37].

In the limiting case $\alpha \to 0$, $r \to \infty$ such that $r\alpha = d$, the wedge geometry tends to two parallel plates separated by a distance d, so we can find the decay rates of an excited atom in this case by taking the limit of the wedge results. Using Eqs. (A16) and (A15), the results for the parallel and perpendicular polarizations are depicted in Figs. 6 and 7, respectively, in terms of the dimensionless variables $\frac{y_0}{\lambda}$ and $\frac{d}{\lambda}$, where $y = r\sin\theta_0 \to r\theta_0$ denotes the distance to the lower plate, d is the distance between the plates, and λ is the transition wavelength. For the case of parallel polarization, a strong suppression occurs for $\frac{d}{\lambda} < \frac{1}{2}$ since the decay rate is proportional to the density of modes in free space and in a cavity formed by two infinite conducting plates, the mode density for the electric field parallel to the surface vanishes for $\frac{d}{\lambda} < \frac{1}{2}$ [38].

In Figs. 6(a) and 7(a) the two curves are analogous in the sense that both are symmetric with respect to the equidistant point to the plates. However, there is a remarkable difference since the regions of enhancement of the former correspond to regions of suppression of the latter and vice versa. Also in Figs. 6(b) and 7(b), the distances between successive peaks for $\frac{\Gamma_\parallel}{\Gamma_0}$ and local minima of $\frac{\Gamma_\perp}{\Gamma_0}$ are λ. These results are in agreement with those reported in [37,38]. Again a comparison of the results depicted in Fig. 6(b) with the experimental data reported in [28] for a classical dipole antenna is interesting.

V. CONDUCTING HALF SHEET

A. Green's tensor

To find the decay rate and energy-level shifts of an atom near a conducting half sheet, let us consider the geometry depicted in Fig. 8. The conducting half sheet is defined by the xz plane for $x \geqslant 0$. For this geometry, the electric-type dyadic

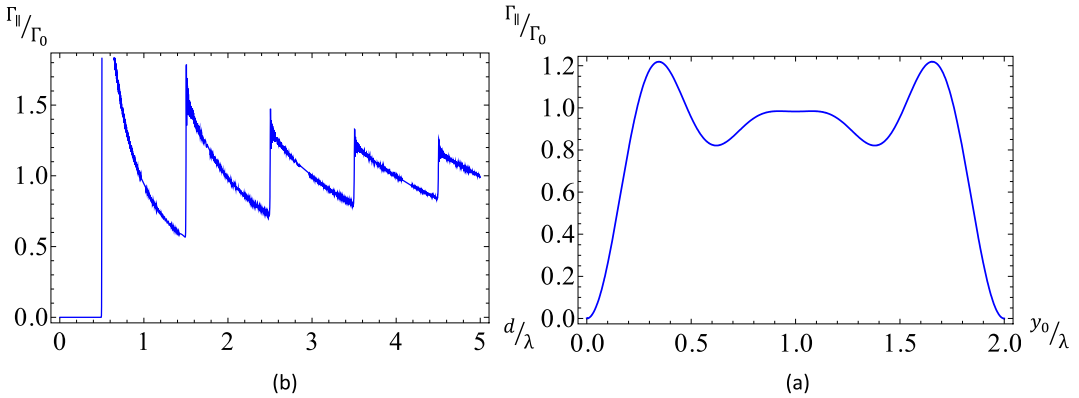

FIG. 6. (Color online) Dimensionless decay rate for parallel polarization of the excited atom between conducting plates in terms of the dimensionless variables (b) $\frac{d}{\lambda}$ and (a) $\frac{y_0}{\lambda}$.

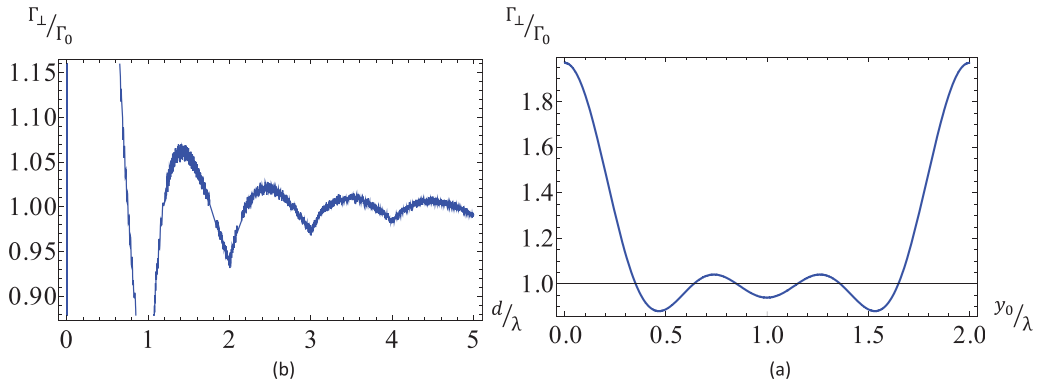

FIG. 7. (Color online) Dimensionless decay rate for perpendicular polarization of the excited atom between conducting plates in terms of the dimensionless variables (b) $\frac{d}{\lambda}$ and (a) $\frac{y_0}{\lambda}$.

Green's function or Green's tensor $\mathscr{D}_{e1}$, satisfying boundary conditions on the walls, is given in Appendix C.

B. Decay rate

To find $\Gamma_\perp$ (Γ_y in our notation) and the in-plane polarizations Γ_x or Γ_z, we need the diagonal components of the Green's tensor. The calculations are straightforward and are given in Appendix C. The decay rates for these two polarizations in terms of the dimensionless distance $\frac{r_0}{\lambda}$ along the curves a, $\theta_0 = \frac{\pi}{50}$; b, $\theta_0 = \frac{\pi}{2}$; and c, $\theta_0 = \frac{5\pi}{6}$ are depicted in Figs. 9(b) and 10(b). The decay rates in terms of θ for fixed distances are also depicted in Figs. 9(a) and 10(a), showing a symmetrical behavior around $\theta_0 = \pi$, as expected. It is interesting to note that in these figures, the presence of the half sheet affects the decay rate only for angles $\theta_0 < \pi/2$ or $\theta_0 > 3\pi/2$; this is because the emitted photon from the excited atom inside the angle $\pi/2 < \theta_0 < 3\pi/2$ cannot be reflected back to the atom.

Let us as a consistency check find the limiting case where the atom is placed at a distance far from the z axis or the edge of the half sheet (see Fig. 8), where d is fixed and $h \to \infty$. In this limiting case using Eqs. (C12)–(C14) and (A10), we will find

$$\frac{\Gamma_y}{\Gamma_0} = -\frac{3}{4q}\left[\left(1+\frac{1}{q^2}\frac{\partial}{\partial y'}\frac{\partial}{\partial y'}\right)\left(\frac{-2\sin(qr_r)}{r_r}\right)+\left(1+\frac{1}{q^2}\frac{\partial}{\partial y'}\frac{\partial}{\partial y'}\right)\left(\frac{-2\sin(qr_i)}{r_i}\right)\right]\Bigg|_{x\to x',y\to y',z\to z'}, \tag{26}$$

$$\frac{\Gamma_x}{\Gamma_0} = \frac{3}{4q}\left[\left(1+\frac{1}{q^2}\frac{\partial}{\partial x'}\frac{\partial}{\partial x'}\right)\left(\frac{-2\sin(qr_r)}{r_r}\right)-\left(1+\frac{1}{q^2}\frac{\partial}{\partial x'}\frac{\partial}{\partial x'}\right)\left(\frac{-2\sin(qr_i)}{r_i}\right)\right]\Bigg|_{x\to x',y\to y',z\to z'}, \tag{27}$$

$$\frac{\Gamma_z}{\Gamma_0} = \frac{3}{4q}\left[\left(1+\frac{1}{q^2}\frac{\partial}{\partial z'}\frac{\partial}{\partial z'}\right)\left(\frac{-2\sin(qr_r)}{r_r}\right)-\left(1+\frac{1}{q^2}\frac{\partial}{\partial z'}\frac{\partial}{\partial z'}\right)\left(\frac{-2\sin(qr_i)}{r_i}\right)\right]\Bigg|_{x\to x',y\to y',z\to z'}. \tag{28}$$

By taking the derivatives and evaluating the expressions at $\mathbf{r}' = \mathbf{r}$, we finally find

$$\frac{\Gamma_y}{\Gamma_0} = 1 - 3\left[\frac{\cos(2qd)}{(2qd)^2} - \frac{\sin(2qd)}{(2qd)^3}\right] \tag{29}$$

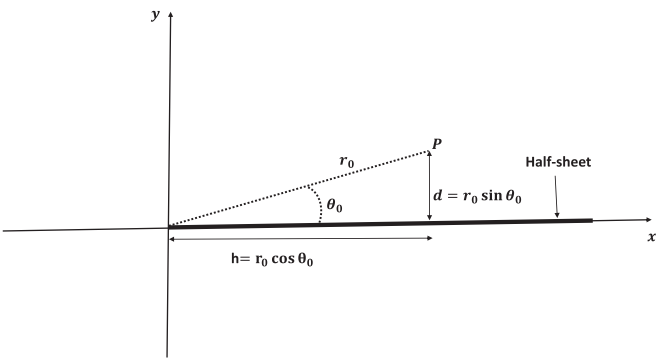

FIG. 8. Geometry of a conducting half sheet.

and

$$\frac{\Gamma_x}{\Gamma_0} = \frac{\Gamma_z}{\Gamma_0} = 1 - \frac{3}{2}\left[\frac{\sin(2qd)}{2qd} + \frac{\cos(2qd)}{(2qd)^2} - \frac{\sin(2qd)}{(2qd)^3}\right], \tag{30}$$

which are the same results reported in [24] for an ideal conducting plane, as expected. As another consistency check let us find the Casimir force on the atom when it is polarized perpendicular to the half sheet and directly above the edge. When the atom is polarizable only in the y direction (see Fig. 8), the only component of the Green's dyadic that contributes is the yy component. We insert this component into Eq. (24) and the result of a straightforward calculation at $\theta = \pi$ leads to

$$\langle \mathbf{E}^2 \rangle = \langle E_y^2 \rangle = 0. \tag{31}$$

This means that when the atom is polarized perpendicular to the half sheet and located exactly above the edge of the half sheet, there is no force on the atom, in agreement with the result reported in [39].

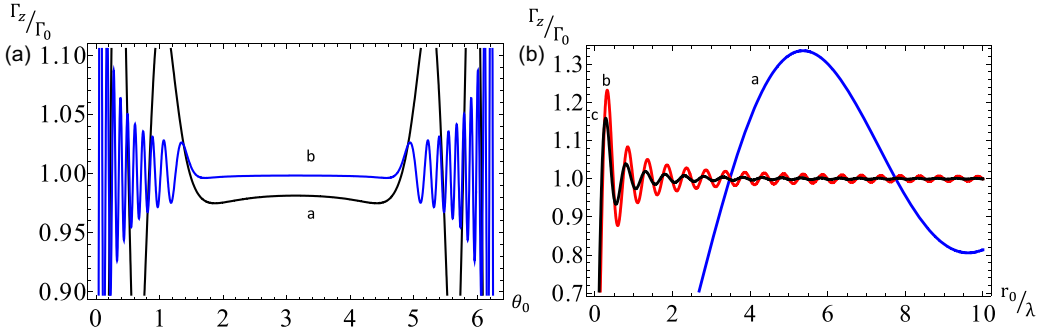

FIG. 9. (Color online) Dimensionless decay rate $\frac{\Gamma_z}{\Gamma_0}$ of an excited atom in the vicinity of a half sheet (a) in terms of the angle $\theta_0 \in (0,2\pi)$ for fixed distances $\frac{r_0}{\lambda} = 1$ (curve a) and $\frac{r_0}{\lambda} = 5$ (curve b) and (b) along the lines $\theta_0 = \frac{\pi}{50}$ (curve a), $\theta_0 = \frac{\pi}{2}$ (curve b), and $\theta_0 = \frac{5\pi}{6}$ (curve c).

C. Energy-level shifts

The energy-level shift of an atom in the presence of an ideal conducting half sheet is

$$\frac{\Delta E_n}{\Delta E_n^0} = \frac{1}{4\ln\frac{mc}{\hbar\gamma}} \int_0^{\frac{mc}{\hbar}} \frac{dq}{q^2+\gamma^2} A, \tag{32}$$

where A is given in Appendix D. The above expression for the energy-level shift cannot be reduced any further to a simple analytical form and one should invoke numerical calculations. As before, when d is fixed and $h \to \infty$ (see Fig. 8), the last three terms in Eq. (D1) vanish and we find

$$\frac{\Delta E_n}{\Delta E_n^0} = 1 - \left(\ln\frac{mc}{\hbar\gamma}\right)^{-1} \int_0^{\frac{mc}{\hbar}} \frac{qdq}{q^2+\gamma^2} \left[\frac{\sin(2qd)}{(2qd)} + 2\frac{\cos(2qd)}{(2qd)^2} - 2\frac{\sin(2qd)}{(2qd)^3}\right], \tag{33}$$

again in agreement with the result reported in [24], as expected.

VI. CONCLUSION

Explicit expressions for the decay rate and energy-level shifts of an atom in the presence of an ideal conducting wedge, two conducting parallel plates, and a half sheet have been obtained in the framework of the canonical quantization approach. The angular and radial dependences of the decay rate for different atomic polarizations of an excited atom and also of the energy-level shifts were depicted and discussed. The consistency of the present approach in some limiting cases was investigated by comparing the relevant results obtained here to the previously reported results. For distances from the cusp smaller than a certain value determined by the opening angle of the wedge, there are configurations for which the atom will not decay at all. This is more clearly understood for the case of conducting parallel plates where, for the case of a transition dipole moment parallel to the plates, a strong suppression occurs for $\frac{d}{\lambda} < \frac{1}{2}$ since the mode density for the electric field parallel to the surface vanishes for $\frac{d}{\lambda} < \frac{1}{2}$. The appearance of enhancement or inhibition of the emission depends not only on the dipole location of the atom but also on the dipole orientational of the atom and the opening angle of the wedge. This study open the way to devising cavity quantum electrodynamics systems, such as the storage, processing, and retrieval of quantum bits for practical realization of quantum information processing [19].

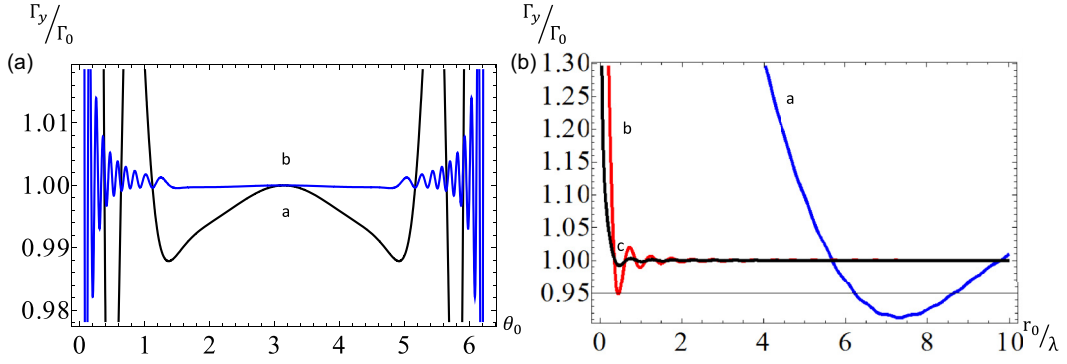

FIG. 10. (Color online) Dimensionless decay rate $\frac{\Gamma_y}{\Gamma_0}$ of an excited atom in the vicinity of a half sheet (a) in terms of the angle $\theta \in (0,2\pi)$ for fixed distances $\frac{r_0}{\lambda} = 1$ (curve a) and $\frac{r_0}{\lambda} = 5$ (curve b) and (b) along the lines $\theta_0 = \frac{\pi}{50}$ (curve a), $\theta_0 = \frac{\pi}{2}$ (curve b), and $\theta_0 = \frac{5\pi}{6}$ (curve c).

APPENDIX A

The diagonal components $\mathscr{D}_{rr}$, $\mathscr{D}_{\theta\theta}$, and $\mathscr{D}_{zz}$ of the Green's tensor in the presence of a perfect conducting wedge are given by [31–33]

$$\begin{aligned}
\mathscr{D}_{rr} &= \frac{-2ip}{q^3}\int_{-\infty}^{+\infty} dk\, e^{ik(z-z')}\sum_{m=0}^{\acute{\infty}}\left[\frac{q^2m^2p^2}{\eta^2rr'}J_{mp}(\eta r)H^{(1)}_{mp}(\eta r') + k^2 J'_{mp}(\eta r)H'^{(1)}_{mp}(\eta r')\right]\sin(mp\theta)\sin(mp\theta') \\
&= \frac{-2ip}{q^3}\left[\frac{1}{rr'}\frac{\partial}{\partial\theta}\frac{\partial}{\partial\theta'}\int_{-\infty}^{+\infty}\frac{q^2dk}{\eta^2}e^{ik(z-z')}\sum_{m=0}^{\acute{\infty}}J_{mp}(\eta r)H^{(1)}_{mp}(\eta r')\cos(mp\theta)\cos(mp\theta')\right. \\
&\quad \left. + \frac{\partial}{\partial r}\frac{\partial}{\partial r'}\int_{-\infty}^{+\infty}\frac{k^2dk}{\eta^2}e^{ik(z-z')}\sum_{m=0}^{\acute{\infty}}J_{mp}(\eta r)H^{(1)}_{mp}(\eta r')\sin(mp\theta)\sin(mp\theta')\right] \\
&= \frac{-ip}{q^3}\left[\frac{1}{rr'}\frac{\partial}{\partial\theta}\frac{\partial}{\partial\theta'}\int_{-\infty}^{+\infty}\frac{q^2dk}{\eta^2}e^{ik(z-z')}\sum_{m=0}^{\acute{\infty}}J_{mp}(\eta r)H^{(1)}_{mp}(\eta r')\{\cos[mp(\theta+\theta')]+\cos[mp(\theta-\theta')]\}\right. \\
&\quad \left. + \frac{\partial}{\partial r}\frac{\partial}{\partial r'}\int_{-\infty}^{+\infty}\frac{k^2dk}{\eta^2}e^{ik(z-z')}\sum_{m=0}^{\acute{\infty}}J_{mp}(\eta r)H^{(1)}_{mp}(\eta r')\{\cos[mp(\theta-\theta')]-\cos[mp(\theta+\theta')]\}\right], \qquad \text{(A1)} \\
\mathscr{D}_{\theta\theta} &= \frac{-2ip}{q^3}\int_{-\infty}^{+\infty} dk\, e^{ik(z-z')}\sum_{m=0}^{\acute{\infty}}\left[\frac{k^2m^2p^2}{\eta^2rr'}J_{mp}(\eta r)H^{(1)}_{mp}(\eta r') + q^2 J'_{mp}(\eta r)H'^{(1)}_{mp}(\eta r')\right]\cos(mp\theta)\cos(mp\theta') \\
&= \frac{-2ip}{q^3}\left[\frac{1}{rr'}\frac{\partial}{\partial\theta}\frac{\partial}{\partial\theta'}\int_{-\infty}^{+\infty}\frac{k^2dk}{\eta^2}e^{ik(z-z')}\sum_{m=0}^{\acute{\infty}}J_{mp}(\eta r)H^{(1)}_{mp}(\eta r')\sin(mp\theta)\sin(mp\theta')\right. \\
&\quad \left. + \frac{\partial}{\partial r}\frac{\partial}{\partial r'}\int_{-\infty}^{+\infty}\frac{q^2dk}{\eta^2}e^{ik(z-z')}\sum_{m=0}^{\acute{\infty}}J_{mp}(\eta r)H^{(1)}_{mp}(\eta r')\cos(mp\theta)\cos(mp\theta')\right] \\
&= \frac{-ip}{q^3}\left[\frac{1}{rr'}\frac{\partial}{\partial\theta}\frac{\partial}{\partial\theta'}\int_{-\infty}^{+\infty}\frac{k^2dk}{\eta^2}e^{ik(z-z')}\sum_{m=0}^{\acute{\infty}}J_{mp}(\eta r)H^{(1)}_{mp}(\eta r')\{\cos[mp(\theta-\theta')]-\cos[mp(\theta+\theta')]\}\right. \\
&\quad \left. + \frac{\partial}{\partial r}\frac{\partial}{\partial r'}\int_{-\infty}^{+\infty}\frac{q^2dk}{\eta^2}e^{ik(z-z')}\sum_{m=0}^{\acute{\infty}}J_{mp}(\eta r)H^{(1)}_{mp}(\eta r')\{\cos[mp(\theta+\theta')]+\cos[mp(\theta-\theta')]\}\right], \qquad \text{(A2)} \\
\mathscr{D}_{zz} &= \frac{-2ip}{q^3}\int_{-\infty}^{+\infty} dk\,\eta^2 e^{ik(z-z')}\sum_{m=0}^{\acute{\infty}}J_{mp}(\eta r)H^{(1)}_{mp}(\eta r')\sin(mp\theta)\sin(mp\theta'), \\
&= \frac{-ip}{q^3}\int_{-\infty}^{+\infty} dk\,\eta^2 e^{ik(z-z')}\sum_{m=0}^{\acute{\infty}}J_{mp}(\eta r)H^{(1)}_{mp}(\eta r')\{\cos[mp(\theta-\theta')]-\cos[mp(\theta+\theta')]\}, \qquad \text{(A3)}
\end{aligned}$$

where $p=\pi/\alpha$ is defined for simplicity and $\eta=\sqrt{q^2-k^2}$. We can henceforth set $z=z'$. For the case $\alpha=\pi/n$, where n is a natural number, the parameter p is an integer ($p=n$) and the summation over m can be done using Graf's addition theorem [40]

$$\sum_{n=0}^{p-1}K_0(\zeta R_n) = 2p\sum_{m=0}^{\acute{\infty}}I_{mp}(\zeta r_1)K_{mp}(\zeta r_2)\cos(mp\phi), \qquad \text{(A4)}$$

where

$$R_n = \sqrt{r_1^2+r_2^2-2r_1r_2\cos(\phi+2n\pi/p)}. \qquad \text{(A5)}$$

Therefore, using Eq. (A4) and changing the integration variable $u=k/q$, the diagonal components can be written as

$$\begin{aligned}
\mathscr{D}_{rr} &= \frac{2}{\pi q^2}\left[\frac{1}{rr'}\sum_{n=0}^{p-1}\int_0^{+\infty}\frac{du}{u^2-1}\frac{\partial}{\partial\theta}\frac{\partial}{\partial\theta'}[K_0(\sqrt{u^2-1}qR_1)+K_0(\sqrt{u^2-1}qR_2)]\right. \\
&\quad \left. + \sum_{n=0}^{p-1}\int_0^{+\infty}\frac{u^2du}{u^2-1}\frac{\partial}{\partial r}\frac{\partial}{\partial r'}[K_0(\sqrt{u^2-1}qR_2)-K_0(\sqrt{u^2-1}qR_1)]\right], \qquad \text{(A6)}
\end{aligned}$$

$$\mathscr{D}_{\theta\theta} = \frac{2}{\pi q^2}\Bigg[\frac{1}{rr'}\sum_{n=0}^{p-1}\int_0^{+\infty}\frac{u^2du}{u^2-1}\frac{\partial}{\partial\theta}\frac{\partial}{\partial\theta'}[K_0(\sqrt{u^2-1}qR_2)-K_0(\sqrt{u^2-1}qR_1)]$$

$$+\sum_{n=0}^{p-1}\int_0^{+\infty}\frac{du}{u^2-1}\frac{\partial}{\partial r}\frac{\partial}{\partial r'}[K_0(\sqrt{u^2-1}qR_1)+K_0(\sqrt{u^2-1}qR_2)]\Bigg], \tag{A7}$$

$$\mathscr{D}_{zz} = \frac{2}{\pi}\sum_{n=0}^{p-1}\int_0^{+\infty}du(u^2-1)[K_0(\sqrt{u^2-1}qR_2)-K_0(\sqrt{u^2-1}qR_1)], \tag{A8}$$

where

$$R_1 = \sqrt{r^2+r'^2-2rr'\cos(\theta+\theta'+2n\pi/p)},$$
$$R_2 = \sqrt{r^2+r'^2-2rr'\cos(\theta-\theta'+2n\pi/p)}. \tag{A9}$$

Now using the formula [40]

$$\int_0^{+\infty}dx\frac{K_\nu(\beta\sqrt{x^2+z^2})}{\sqrt{(x^2+z^2)^\nu}}x^{2\mu+1} = \frac{2^\mu\Gamma(\mu+1)}{\beta^{\mu+1}z^{\nu-\mu-1}}K_{\nu-\mu-1}(\beta z) \tag{A10}$$

and doing some straightforward calculations, we finally find the imaginary part of the diagonal components of the Green's tensor as

$$\mathrm{Im}[\mathscr{D}_{rr}(\mathbf{r}_0,\mathbf{r}_0,\omega)] = \sum_{n=0}^{p-1}\Bigg[\left(\frac{\cos x}{x^2}+\frac{\sin x}{x}-\frac{\sin x}{x^3}\right)+\sin^2\left(\frac{n\pi}{p}\right)\left(\frac{\cos x}{x^2}-\frac{\sin x}{x}-\frac{\sin x}{x^3}\right)$$
$$-\left(\frac{\cos x_\theta}{x_\theta^2}+\frac{\sin x_\theta}{x_\theta}-\frac{\sin x_\theta}{x_\theta^3}\right)-\sin^2\left(\theta+\frac{n\pi}{p}\right)\left(\frac{\cos x_\theta}{x_\theta^2}-\frac{\sin x_\theta}{x_\theta}-\frac{\sin x_\theta}{x_\theta^3}\right)\Bigg], \tag{A11}$$

$$\mathrm{Im}[\mathscr{D}_{\theta\theta}(\mathbf{r}_0,\mathbf{r}_0,\omega)] = -\sum_{n=0}^{p-1}\Bigg[2\left(\frac{\cos x}{x^2}-\frac{\sin x}{x^3}\right)-\sin^2\left(\frac{n\pi}{p}\right)\left(\frac{\cos x}{x^2}-\frac{\sin x}{x}-\frac{\sin x}{x^3}\right)$$
$$+2\left(\frac{\cos x_\theta}{x_\theta^2}-\frac{\sin x_\theta}{x_\theta^3}\right)-\sin^2\left(\theta+\frac{n\pi}{p}\right)\left(\frac{\cos x_\theta}{x_\theta^2}-\frac{\sin x_\theta}{x_\theta}-\frac{\sin x_\theta}{x_\theta^3}\right)\Bigg], \tag{A12}$$

$$\mathrm{Im}[\mathscr{D}_{zz}(\mathbf{r}_0,\mathbf{r}_0,\omega)] = \sum_{n=0}^{p-1}\Bigg[\left(\frac{\sin x}{x}+\frac{\cos x}{x^2}-\frac{\sin x}{x^3}\right)-\left(\frac{\sin x_\theta}{x_\theta}+\frac{\cos x_\theta}{x_\theta^2}-\frac{\sin x_\theta}{x_\theta^3}\right)\Bigg], \tag{A13}$$

where $x_\theta = 2r_0q\sin(\theta_0+n\pi/p)$ and $x = 2r_0q\sin(n\pi/p)$. By inserting Eqs. (A11)–(A13) into (13), we find

$$\frac{\Gamma_r}{\Gamma_0} = \frac{3}{2}\sum_{n=0}^{p-1}\Bigg[\left(\frac{\cos x}{x^2}+\frac{\sin x}{x}-\frac{\sin x}{x^3}\right)+\sin^2\left(\frac{n\pi}{p}\right)\left(\frac{\cos x}{x^2}-\frac{\sin x}{x}-\frac{\sin x}{x^3}\right)$$
$$-\left(\frac{\cos x_\theta}{x_\theta^2}+\frac{\sin x_\theta}{x_\theta}-\frac{\sin x_\theta}{x_\theta^3}\right)-\sin^2\left(\theta+\frac{n\pi}{p}\right)\left(\frac{\cos x_\theta}{x_\theta^2}-\frac{\sin x_\theta}{x_\theta}-\frac{\sin x_\theta}{x_\theta^3}\right)\Bigg], \tag{A14}$$

$$\frac{\Gamma_\theta}{\Gamma_0} = -\frac{3}{2}\sum_{n=0}^{p-1}\Bigg[2\left(\frac{\cos x}{x^2}-\frac{\sin x}{x^3}\right)-\sin^2\left(\frac{n\pi}{p}\right)\left(\frac{\cos x}{x^2}-\frac{\sin x}{x}-\frac{\sin x}{x^3}\right)$$
$$+2\left(\frac{\cos x_\theta}{x_\theta^2}-\frac{\sin x_\theta}{x_\theta^3}\right)-\sin^2\left(\theta+\frac{n\pi}{p}\right)\left(\frac{\cos x_\theta}{x_\theta^2}-\frac{\sin x_\theta}{x_\theta}-\frac{\sin x_\theta}{x_\theta^3}\right)\Bigg], \tag{A15}$$

$$\frac{\Gamma_z}{\Gamma_0} = \frac{3}{2}\sum_{n=0}^{p-1}\Bigg[\left(\frac{\sin x}{x}+\frac{\cos x}{x^2}-\frac{\sin x}{x^3}\right)-\left(\frac{\sin x_\theta}{x_\theta}+\frac{\cos x_\theta}{x_\theta^2}-\frac{\sin x_\theta}{x_\theta^3}\right)\Bigg]. \tag{A16}$$

APPENDIX B

Using Eqs. (A11)–(A13), we find

$$\mathrm{Im}\left[\sum_{\alpha}\mathscr{D}_{\alpha\alpha}(\mathbf{r}_0,\mathbf{r}_0,\omega)\right]=\sum_{n=0}^{p-1}2\left[\frac{\sin x}{x}-\sin^2\left(\frac{n\pi}{p}\right)\left(\frac{\sin x}{x}-\frac{\cos x}{x^2}+\frac{\sin x}{x^3}\right)-\left(\frac{\sin x_\theta}{x_\theta}+2\frac{\cos x_\theta}{x_\theta^2}-2\frac{\sin x_\theta}{x_\theta^3}\right)\right]. \tag{B1}$$

By substituting Eq. (B1) into Eq. (22), we find for the energy-level shifts inside the wedge

$$\frac{\Delta E_n}{\Delta E_n^0}=\left(\ln\frac{mc}{\hbar\gamma}\right)^{-1}\sum_{n=0}^{p-1}\int_0^{\frac{mc}{\hbar}}\frac{q\,dq}{q^2+\gamma^2}\left[\frac{\sin x}{x}-\sin^2\left(\frac{n\pi}{p}\right)\left(\frac{\sin x}{x}-\frac{\cos x}{x^2}+\frac{\sin x}{x^3}\right)-\left(\frac{\sin x_\theta}{x_\theta}+2\frac{\cos x_\theta}{x_\theta^2}-2\frac{\sin x_\theta}{x_\theta^3}\right)\right], \tag{B2}$$

which for the special choice $p=1$ tends to the familiar expression for an ideal conducting plane [24].

APPENDIX C

The electric-type Green's tensor $\mathscr{D}_{e1}$ is given by [32,33,36]

$$\begin{aligned}\mathscr{D}_{e1}=&\frac{1}{2q}\left\{\left(I+\frac{\nabla'\nabla'}{q^2}\right)\left[\frac{e^{-iqr_i}}{r_i}-iqI(\zeta_-,r_i)\right]-I_r\left(I+\frac{\nabla'\nabla'}{q^2}\right)\left[\frac{e^{-iqr_r}}{r_r}-iqI(\zeta_+,r_r)\right]\right\}\\&-\frac{i}{q}\left[\hat{x}\sin\left(\frac{\theta}{2}\right)-\hat{y}\cos\left(\frac{\theta}{2}\right)\right]\left\{\left[\hat{x}\sin\left(\frac{\theta'}{2}\right)-\hat{y}\cos\left(\frac{\theta'}{2}\right)\right]\frac{H_0^{(2)}(qp)}{\sqrt{rr'}}+\frac{1}{q}\nabla'\sin\left(\frac{\theta'}{2}\right)\frac{r+r'}{\sqrt{rr'}}\frac{H_1^{(2)}(qp)}{p}\right\},\end{aligned} \tag{C1}$$

where

$$I=\hat{x}\hat{x}+\hat{y}\hat{y}+\hat{z}\hat{z}, \tag{C2}$$

$$I_r=\hat{x}\hat{x}-\hat{y}\hat{y}+\hat{z}\hat{z}, \tag{C3}$$

$$p=\sqrt{(r+r')^2+(z-z')^2}, \tag{C4}$$

$$r_i=\sqrt{(x-x')^2+(y-y')^2+(z-z')^2}=\sqrt{r^2+r'^2-2rr'\cos(\theta-\theta')+(z-z')^2}, \tag{C5}$$

$$r_r=\sqrt{(x-x')^2+(y+y')^2+(z-z')^2}=\sqrt{r^2+r'^2-2rr'\cos(\theta+\theta')+(z-z')^2}, \tag{C6}$$

$$I(\zeta,\eta)=\int_0^{\zeta}dt\,\frac{H_1^{(2)}(\omega\sqrt{t^2+\eta^2})}{\sqrt{t^2+\eta^2}}, \tag{C7}$$

and $\zeta_\mp=2\sqrt{rr'}\cos(\frac{\theta\mp\theta'}{2})$. By making use of Eq. (C1), we find the diagonal components of the Green's tensor as

$$\begin{aligned}\mathscr{D}_{yy}=&\frac{1}{2q}\left[\left(1+\frac{1}{q^2}\frac{\partial}{\partial y'}\frac{\partial}{\partial y'}\right)\left(\frac{e^{-iqr_i}}{r_i}-iqI(\zeta_-,r_i)\right)+\left(1+\frac{1}{q^2}\frac{\partial}{\partial y'}\frac{\partial}{\partial y'}\right)\left(\frac{e^{-iqr_r}}{r_r}-iqI(\zeta_+,r_r)\right)\right]\\&-\frac{i}{q}\left\{\cos\left(\frac{\theta}{2}\right)\cos\left(\frac{\theta'}{2}\right)\frac{J_0(qp)}{\sqrt{rr'}}-\frac{1}{q}\cos\left(\frac{\theta}{2}\right)\frac{\partial}{\partial y'}\left[\sin\left(\frac{\theta'}{2}\right)\frac{r+r'}{\sqrt{rr'}}\frac{J_1(qp)}{p}\right]\right\},\end{aligned} \tag{C8}$$

$$\begin{aligned}\mathscr{D}_{xx}=&\frac{1}{2q}\left[\left(1+\frac{1}{q^2}\frac{\partial}{\partial x'}\frac{\partial}{\partial x'}\right)\left(\frac{e^{-iqr_i}}{r_i}-iqI(\zeta_-,r_i)\right)-\left(1+\frac{1}{q^2}\frac{\partial}{\partial x'}\frac{\partial}{\partial x'}\right)\left(\frac{e^{-iqr_r}}{r_r}-iqI(\zeta_+,r_r)\right)\right]\\&-\frac{i}{q}\left\{\sin\left(\frac{\theta}{2}\right)\sin\left(\frac{\theta'}{2}\right)\frac{J_0(qp)}{\sqrt{rr'}}+\frac{1}{q}\sin\left(\frac{\theta}{2}\right)\frac{\partial}{\partial x'}\left[\sin\left(\frac{\theta'}{2}\right)\frac{r+r'}{\sqrt{rr'}}\frac{J_1(qp)}{p}\right]\right\},\end{aligned} \tag{C9}$$

$$\mathscr{D}_{zz}=\frac{1}{2q}\left[\left(1+\frac{1}{q^2}\frac{\partial}{\partial z'}\frac{\partial}{\partial z'}\right)\left(\frac{e^{-iqr_i}}{r_i}-iqI(\zeta_-,r_i)\right)-\left(1+\frac{1}{q^2}\frac{\partial}{\partial z'}\frac{\partial}{\partial z'}\right)\left(\frac{e^{-iqr_r}}{r_r}-iqI(\zeta_+,r_r)\right)\right]. \tag{C10}$$

To calculate Γ_y, we need the yy component of the Green's tensor. Therefore, by inserting Eq. (C8) into Eq. (13), we find

$$\begin{aligned}\frac{\Gamma_y}{\Gamma_0}=&-\frac{3}{4q}\mathrm{Im}\left(\left[\left(1+\frac{1}{q^2}\frac{\partial}{\partial y'}\frac{\partial}{\partial y'}\right)\left(\frac{e^{-iqr_r}}{r_r}-iqI(\zeta_+,r_r)\right)+\left(1+\frac{1}{q^2}\frac{\partial}{\partial y'}\frac{\partial}{\partial y'}\right)\left(\frac{e^{-iqr_i}}{r_i}-iqI(\zeta_-,r_i)\right)\right]\right.\\&\left.-2i\left\{\cos\left(\frac{\theta}{2}\right)\cos\left(\frac{\theta'}{2}\right)\frac{J_0(qp)}{\sqrt{rr'}}-\frac{1}{q}\cos\left(\frac{\theta}{2}\right)\frac{\partial}{\partial y'}\left[\sin\left(\frac{\theta'}{2}\right)\frac{r+r'}{\sqrt{rr'}}\frac{J_1(qp)}{p}\right]\right\}\right)\Big|_{x\to x',y\to y',z\to z'}\end{aligned} \tag{C11}$$

and for the in-plane polarizations Γ_x or Γ_z, we find

$$\frac{\Gamma_x}{\Gamma_0}=\frac{3}{4q}\mathrm{Im}\Bigg(\Bigg[\left(1+\frac{1}{q^2}\frac{\partial}{\partial x'}\frac{\partial}{\partial x'}\right)\left(\frac{e^{-iqr_r}}{r_r}-iqI(\zeta_+,r_r)\right)-\left(1+\frac{1}{q^2}\frac{\partial}{\partial x'}\frac{\partial}{\partial x'}\right)\left(\frac{e^{-iqr_i}}{r_i}-iqI(\zeta_-,r_i)\right)\Bigg]$$
$$+2i\left\{\sin\left(\frac{\theta}{2}\right)\sin\left(\frac{\theta'}{2}\right)\frac{J_0(qp)}{\sqrt{rr'}}+\frac{1}{q}\sin\left(\frac{\theta}{2}\right)\frac{\partial}{\partial x'}\left[\sin\left(\frac{\theta'}{2}\right)\frac{r+r'}{\sqrt{rr'}}\frac{J_1(qp)}{p}\right]\right\}\Bigg)\Bigg|_{x\to x',y\to y',z\to z'}, \tag{C12}$$

$$\frac{\Gamma_z}{\Gamma_0}=\frac{3}{4q}\mathrm{Im}\left[\left(1+\frac{1}{q^2}\frac{\partial}{\partial z'}\frac{\partial}{\partial z'}\right)\left(\frac{e^{-iqr_r}}{r_r}-iqI(\zeta_+,r_r)\right)-\left(1+\frac{1}{q^2}\frac{\partial}{\partial z'}\frac{\partial}{\partial z'}\right)\left(\frac{e^{-iqr_i}}{r_i}-iqI(\zeta_-,r_i)\right)\right]\Bigg|_{x\to x',y\to y',z\to z'}. \tag{C13}$$

Using Eqs. (C11) and (C13) and doing straightforward calculations, we find

$$\frac{\Gamma_y}{\Gamma_0}=\frac{1}{2}-\frac{3}{2}\Bigg[\frac{\cos(2y_0q)}{(2y_0q)^2}-\frac{\sin(2y_0q)}{(2y_0q)^3}+\left(2\cos(\theta_0/2)\cos(3\theta_0/2)-\frac{\cos(\theta_0)}{2}-\frac{\cos(2\theta_0)}{2}+\frac{\sin^2(\theta_0)}{2}\right)\frac{J_1(2r_0q)}{(2r_0q)^2}$$
$$-\left(\frac{\sin^2(\theta_0)}{4}\right)\frac{J_2(2r_0q)}{2r_0q}-\left(2\cos^4(\theta_0/2)+\frac{\sin^2(\theta_0)}{4}\right)\frac{J_0(2r_0q)}{2r_0q}-\frac{1}{2}\int_0^{2r_0q}dx\left(\frac{J_1(x)}{x}-\frac{J_2(x)}{x^2}\right)$$
$$-\frac{1}{2}\int_0^{2r_0q\cos(\theta_0)}dx\frac{z^3J_0(z)-[2z^2+(2y_0q)^2z^2-z^4]J_1(z)+4(2y_0q)^2zJ_2(z)}{z^5}\Bigg], \tag{C14}$$

$$\frac{\Gamma_z}{\Gamma_0}=\frac{1}{2}-\frac{3}{4}\Bigg[\frac{\sin(2y_0q)}{(2y_0q)}+\frac{\cos(2y_0q)}{(2y_0q)^2}-\frac{\sin(2y_0q)}{(2y_0q)^3}+\int_0^{2r_0q\cos(\theta_0)}dx\left(\frac{J_1(z)}{z}-\frac{J_1(z)}{z^3}+\frac{J_0(z)}{2z^2}-\frac{J_2(z)}{2z^2}\right)$$
$$-\int_0^{2r_0q}dx\left(\frac{J_1(x)}{x}-\frac{J_1(x)}{x^3}+\frac{J_0(x)}{2x^2}-\frac{J_2(x)}{2x^2}\right)\Bigg], \tag{C15}$$

where $y_0=r_0\sin\theta_0$ and $z=\sqrt{x^2+(2y_0q)^2}$.

APPENDIX D

By inserting Eqs. (C8)–(C10) into Eq. (15), we find Eq. (32), where

$$A=\mathrm{Im}\Bigg(\left[1+\frac{1}{q^2}\left(\frac{\partial}{\partial x'}\frac{\partial}{\partial x'}-\frac{\partial}{\partial y'}\frac{\partial}{\partial y'}+\frac{\partial}{\partial z'}\frac{\partial}{\partial z'}\right)\right]\left[\frac{e^{-iqr_r}}{r_r}-iqI(\zeta_+,r_r)\right]$$
$$-\left[3+\frac{1}{q^2}\left(\frac{\partial}{\partial x'}\frac{\partial}{\partial x'}+\frac{\partial}{\partial y'}\frac{\partial}{\partial y'}+\frac{\partial}{\partial z'}\frac{\partial}{\partial z'}\right)\right]\left[\frac{e^{-iqr_i}}{r_i}-iqI(\zeta_-,r_i)\right]$$
$$+2i\left\{\cos\left(\frac{\theta-\theta'}{2}\right)\frac{J_0(qp)}{\sqrt{rr'}}+\frac{1}{q}\sin\left(\frac{\theta}{2}\right)\frac{\partial}{\partial x'}\left[\sin\left(\frac{\theta'}{2}\right)\frac{r+r'}{\sqrt{rr'}}\frac{J_1(qp)}{p}\right]\right.$$
$$\left.-\frac{1}{q}\cos\left(\frac{\theta}{2}\right)\frac{\partial}{\partial y'}\left[\sin\left(\frac{\theta'}{2}\right)\frac{r+r'}{\sqrt{rr'}}\frac{J_1(qp)}{p}\right]\right\}\Bigg)\Bigg|_{x\to x',y\to y',z\to z'}. \tag{D1}$$

[1] W. Vogel and D.-G. Welsch, *Quantum Optics* (Wiley-VCH, Berlin, 2006).
[2] G. S. Agarwal, Phys. Rev. A **11**, 230 (1975); **11**, 243 (1975); **11**, 253 (1975); **12**, 1475 (1975); **12**, 1974 (1975); **12**, 1987 (1975).
[3] B. Huttner and S. M. Barnett, Phys. Rev. A **46**, 4306 (1992).
[4] F. Kheirandish and M. Amooshahi, Phys. Rev. A **74**, 042102 (2006); M. Amooshahi and F. Kheirandish, *ibid.* **76**, 062103 (2007).
[5] F. Kheirandish, M. Amooshahi, and M. Soltani, J. Phys. B **42**, 075504 (2009).
[6] F. Kheirandish and M. Soltani, Phys. Rev. A **78**, 012102 (2008).
[7] K. A. Milton, *The Casimir Effect: Physical Manifestations of Zero-Point Energy* (World Scientific, Singapore, 2001).
[8] M. Babiker and G. Barton, Proc. R. Soc. London Ser. A **326**, 255 (1972); **326**, 277 (1972).
[9] G. Barton, J. Phys. B **7**, 2134 (1974).
[10] G. Barton, Proc. R. Soc. London Ser. A **410**, 175 (1987).
[11] D. Meschede, W. Jhe, and E. A. Hinds, Phys. Rev. A **41**, 1587 (1990).
[12] M. R. Philpott, Chem. Phys. Lett. **19**, 435 (1973).
[13] F. Kheirandish and S. Salimi, Phys. Rev. A **84**, 062122 (2011).
[14] G. Barton, Proc. R. Soc. London Ser. A **320**, 251 (1970).
[15] G. Barton, Proc. R. Soc. London Ser. A **410**, 141 (1987).
[16] F. S. S. Rosa, T. N. C. Mendes, A. Tenório, and C. Farina, Phys. Rev. A **78**, 012105 (2008).
[17] H. J. Zhao and M. L. Du, J. Phys. B **44**, 025401 (2011).
[18] S. C. Skipsey, M. Al-Amri, M. Babiker, and G. Juzeliūnas, Phys. Rev. A **73**, 011803(R) (2006).
[19] D. Bouwmeester, A. Ekret, and A. Zeilinger, *The Physics of Quantum Information* (Springer, Berlin, 2000).

[20] I. Brevik, M. Lygren, and V. N. Marachevsky, Ann. Phys. (NY) **267**, 134 (1998).
[21] L. L. DeRaad, Jr., and K. A. Milton, Ann. Phys. (NY) **136**, 229 (1981).
[22] J. Schwinger, L. L DeRaad, Jr., and K. A. Milton, Ann. Phys. (NY) **115**, 1 (1978); K. A. Milton, L. L. DeRaad, Jr., and J. Schwinger, *ibid.* **115**, 388 (1978).
[23] T. G. Philbin, C. Xiong, and U. Leonhardt, Ann. Phys. (NY) **325**, 579 (2010).
[24] R. Matloob, Phys. Rev. A **62**, 022113 (2000).
[25] L. D. Landau and E. M. Lifshitz, *Statistical Physics* (Pergamon, Oxford, 1980), Pt. 2.
[26] L. Novotny and B. Hecht, *Principles of Nano-Optics* (Cambridge University Press, Cambridge, 2006).
[27] L. R. Fleet, M. Babiker, and M. I. J. Probert, Eur. J. Phys. **30**, S81 (2009).
[28] F. B. Seeley, J. E. Alexander, R. W. Connatser, J. S. Conway, and J. P. Dowling, Am. J. Phys. **61**, 545 (1993).
[29] W. Greiner, B. Mller, and J. Rafelski, *Quantum Electrodynamics of Strong Fields* (Springer, Berlin, 1985).
[30] J. M. Wylie and J. E. Sipe, Phys. Rev. A **32**, 2030 (1985).
[31] I. Brevik and M. Lygren, Ann. Phys. (NY) **251**, 157 (1996).
[32] C.-T. Tai, *Dyadic Green's Functions in Electromagnetic Theory* (Intext, Scranton, 1971).
[33] C.-T. Tai, Eigen-function expansion of dyadic Green's function, University of Michigan Radiation Laboratory Report No. 28, 1973 (unpublished).
[34] K. A. Milton, E. K. Abalo, P. Parashar, N. Pourtolami, I. Brevik, and S. A Ellingsen, Phys. Rev. A **83**, 062507 (2011).
[35] C. I. Sukenik, M. G. Boshier, D. Cho, V. Sandoghdar, and E. A. Hinds, Phys. Rev. Lett. **70**, 560 (1993).
[36] K. Sawaya, T. Ishizone, and Y. Mushiake, Proc. IEEE **AP-29**, 749 (1981).
[37] R. G. Hulet, E. S. Hilfer, and D. Kleppner, Phys. Rev. Lett. **55**, 2137 (1985).
[38] D. T. Alves, C. Farina, and A. C. Tort, Phys. Rev. A **61**, 034102 (2000).
[39] C. Eberlein and R. Zietal, Phys. Rev. A **80**, 012504 (2009).
[40] I. S. Gradshteyn and I. M. Ryzhik, *Table of Integrals, Series, and Products* (Academic, London, 1980).